Dalton Transactions

ROYAL SOCIETY OF CHEMISTRY

PAPER

Published on 17 July 2026

Cite this: DOI: 10.1039/d6dt01324d

Lanthanum and gadolinium complexes with neutral tertiary phosphine ligands: synthesis, structures, magnetism and bonding

Jan Locher, †[a] Sophie Jana Gross,[a] Christian Zacharias,[b] Sebastian Dechert,[a] Serhiy Demeshko[a] and Lisa Vondung *[a,b]

Lanthanum and gadolinium complexes with neutral bidentate phosphine ligands and cyclopentadienyl (Cp^-) or dianionic cyclooctatetraene (COT^{2-}) ligands were investigated. Solvent-free precursors [Ln(COT)I] and $LnCp_3$ (Ln = La, Gd) were reacted with the bisphosphines 1,2-bis(dimethylphosphino)ethane (dmpe) and bis(dimethylphosphino)methane (dmpm). The resulting complexes [Gd(COT)I(dmpe)], $[\{Gd(COT)(\mu\text{-}I)\}_2(\mu\text{-}dmpm)]$, $[\{LnCp_3\}_2(\mu\text{-}dmpe)]$ (Ln = La, Gd) and the precursor $[Gd(COT)I(thf)_2]$ were crystallographically characterised. Depending on the ancillary ligands and bisphosphine backbone, chelating and bridging coordination modes were observed for the bisphosphine ligands. The magnetism of the dimeric gadolinium complexes was investigated *via* SQUID magnetometry. A weak antiferromagnetic coupling was found between the Gd^{3+} ions in $[\{Gd(COT)(\mu\text{-}I)\}_2(\mu\text{-}dmpm)]$. Quantum chemical bonding analysis using Quantum Theory of Atoms in Molecules showed a correlation between the (overall small) bond covalency and the Ln-P bond length.

Received 1st June 2026,
Accepted 17th July 2026

DOI: 10.1039/d6dt01324d

rsc.li/dalton

Introduction

Tertiary phosphine ligands (PR_3) are omnipresent in the chemistry of transition metals, especially in catalysis.[1,2] The substituents at P can be easily varied to adjust the steric and electronic properties of the phosphine. With bidentate phosphine ligands, chirality can be introduced, which is key for enantioselective catalysts and applied in industrial processes.[3] Therefore, a large range of different phosphine ligands are easily available, either commercially or synthetically. In lanthanoid complexes, however, neutral phosphine ligands remain scarce. While the first example, $[YbCp_3(PPh_3)]$, was reported in 1965,[4,5] it took another 18 years for the first crystal structure of this compound class to be reported. UV/Vis and NMR-spectroscopic studies of $[YbCp_3(PRR'_2)]$ (R = H, Cy, Ph, R′ = Me, Cy, Ph) and $[YbCp^*_2(PR_3)]$ (R = Me, Et) complexes suggested a high lability especially of monodentate phosphine ligands, which can be attributed to the mismatch of the hard Lewis acidic lanthanoid ions with the soft Lewis basic phosphine ligands according to the HSAB concept.[6,7] Anchoring the phosphines to anionic and hard Lewis bases, such as amides, to form multidentate ligands, has proven successful in stabilising a variety of lanthanoid complexes with phosphine donor groups. A variety of these mixed donor group PN-, PNP-, PO- and other multidentate ligands has been established for various lanthanoids (Fig. 1a).[8–16] These ligand frameworks were also demonstrated to support a variety of reactivity such as the formation of heterobimetallic complexes or as catalysts in polymerisation reactions.[17–21]

Neutral phosphine ligands without an anionic donor group, however, were largely ignored in the further development of lanthanoid coordination chemistry. Of the 160 reported crystal structures in the CCDC database with an Ln-PR_3 motif, only 12 complexes and one cluster contain non-anchored neutral tertiary phosphines (Fig. 1b).[22–31] For some of the lanthanoids, such as gadolinium, none have been reported so far. In a more recent study, Rinehart and co-workers showed that by employing different phosphine ligands the structure of a series of erbium complexes with cyclooctatetraene dianion ($(C_8H_8)^{2-}$ = COT^{2-}) ligands could be tuned, impacting their magnetic properties.[29] Apart from this, further systematic studies into the trends in structures, bonding and lability of lanthanoid phosphine complexes are lacking. Therefore, we set out to gain more insights into this underexplored ligand class. In this first study, we chose an early (La) and a mid-series (Gd) lanthanoid to compare potential size effects. As supporting ligands, COT^{2-} and cyclopenta-

[a]University of Göttingen, Institute of Inorganic Chemistry, Tammannstraße 4, 37077 Göttingen, Germany
[b]University of Hamburg, Department of Chemistry, Martin-Luther-King-Platz 6, 20146 Hamburg, Germany. E-mail: lisa.vondung@uni-hamburg.de
†Current address: Karlsruhe Institute of Technology, Institute for Inorganic Chemistry, Engesserstraße 15, 76131 Karlsruhe, Germany.

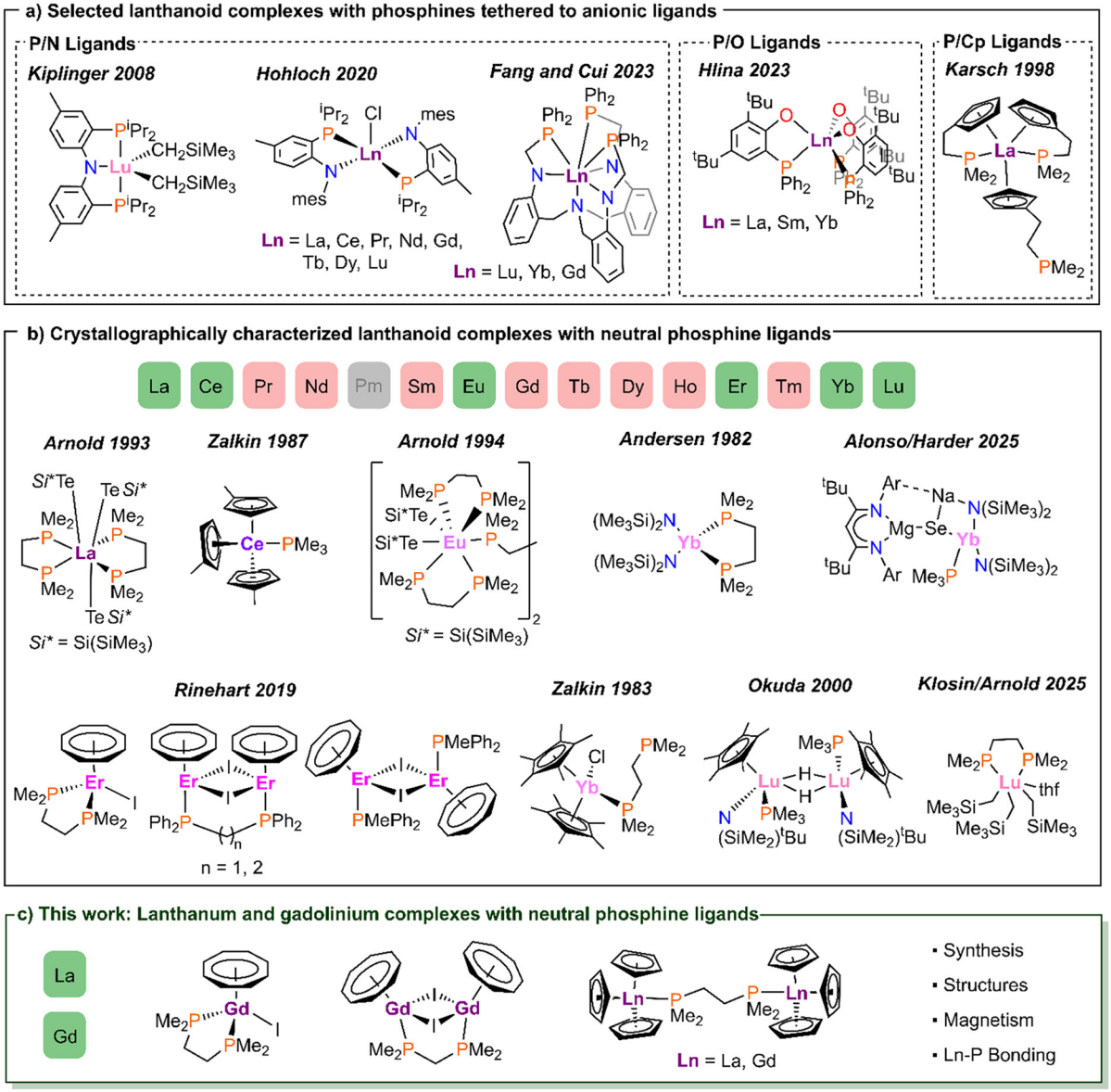

Fig. 1 (a) Selected examples of lanthanoid complexes supported by multidentate ligands with tertiary phosphines and anionic donor groups. (b) All crystallographically characterised lanthanoid complexes with neutral tertiary phosphine ligands. Colour code for lanthanoids: green: structure reported previously with neutral tertiary phosphine ligands. Red: no structure reported previously with neutral tertiary phosphine ligands. (c) Overview of the scope of this work.

dienide ($(C_5H_5)^-$ = Cp^-) were chosen due to their well-established ability to support a range of organometallic lanthanoid complexes. The bisphosphines 1,2-bis(dimethylphosphino)ethane (dmpe) and 1,2-bis(dimethylphosphino)methane (dmpm) were chosen to allow for comparison of effects of the bite angle and due to the expected higher stability of chelating ligands compared to monodentate PR_3. Since all but three of the previously crystallographically characterised lanthanoid phosphine complexes were obtained using methylphosphines, we chose these, as well as to avoid steric hindrance preventing coordination of the phosphines to the metals.

Results and discussion

Synthesis and characterisation of COT^{2-}-supported lanthanoid complexes

The precursors [Ln(COT)I(thf)$_n$] (Ln = La, Gd, n = 2 (Gd), 3 (La)) were synthesised either in analogy to a procedure initially reported by Nakamura and adapted by Roesky directly from the elements and cyclooctatetraene (for lanthanum) or the isolated lanthanoid iodide and potassium cyclooctatetraenide (for gadolinium) (Scheme 1).[33,34] For the previously unreported complex [Gd(COT)I(thf)$_2$] (**1**), single crystals were

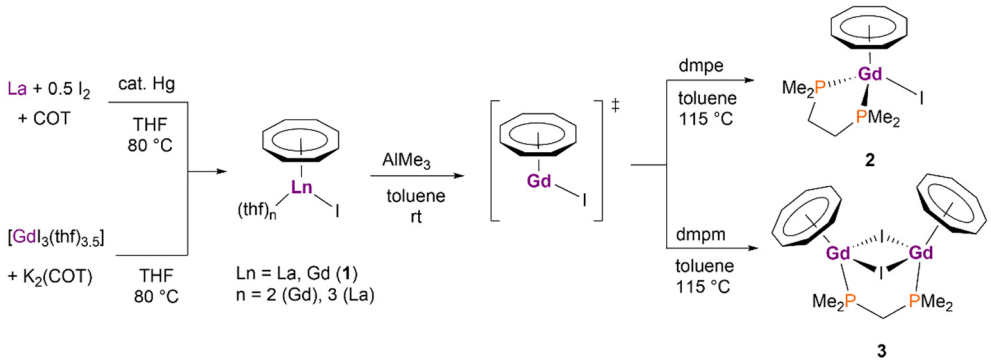

Scheme 1 Synthesis of COT^{2-}-supported gadolinium phosphine complexes **2** and **3** *via* THF abstraction from **1**.

obtained by storing a THF solution at −30 °C (Fig. 2a). Despite repeated attempts, only twinned crystals could be obtained. Nonetheless, a structure determination was possible and showed that **1** crystallises with two molecules in the asymmetric unit and is isostructural to other known heteroleptic COT^{2-}/iodide/THF complexes of the later lanthanoids [Ln(COT)I(thf)$_2$] (Ln = Tb, Dy, Ho, Er, Tm) with a three-legged piano-stool structure.[34–38] The Gd-I (3.077(3)/3.085(3) Å), Gd-$COT_{centroid}$ (1.829(1)/1.870(1) Å) and Gd-O (O1/3: 2.47(2)/2.45(3) Å, O2/4: 2.42(3)/2.39(3) Å) bond lengths are all in the expected ranges.[39–43] In accordance with the smaller ionic radius of Gd^{3+}, only two THF molecules are coordinated, as opposed to three coordinated THF molecules for the larger early lanthanoids La, Ce, Nd and Sm.[44–46] With both precursors at hand, we attempted the *in situ* removal of coordinated THF with $AlMe_3$ following a procedure by Rinehart and co-workers and subsequent complexation reaction with the bidentate phosphine ligands dmpe and dmpm.[29] The initial abstraction of THF was necessary, as a direct reaction of the [La(COT)I(thf)$_3$] precursor with dmpe proved to be not possible, even at elevated temperatures, as observed by NMR. For Yb phosphine complexes similar observations have been reported previously, where THF easily replaced coordinated dmpe.[24] Similarly, it was reported that for the formation of the Lu phosphine complex from a THF containing precursor, a large excess of at least 30 equivalents of phosphine were necessary.[28] For lanthanum, no phosphine coordination was observed *via* ^{1}H and $^{31}P\{^1H\}$ NMR spectroscopy for both the dmpe and dmpm ligand. Additionally, no resonances for [Ln(COT)I] were observed either, as its solubility in toluene-d_8 was too low. Heating the reactions for five days only showed slow decomposition of the precursor complexes through emerging resonances in the ^{1}H NMR spectrum attributed to free cyclooctatetraene. This lack of complexation reactivity can possibly be attributed to the formation of a dimeric La species, which is insoluble in toluene. Mashima, Anwander and co-workers reported the formation of a dimeric lanthanum complex [{La(COT)(thf)$_2$}$_2$(μ-I)$_2$] after reaction of [La(COT)I(thf)$_3$] with $AlMe_3$ in toluene and solvation of the product in THF.[46] They also noted that even in excess THF, the dimer [{La(COT)(thf)$_2$}$_2$(μ-I)$_2$] is stable and no conversion to the monomeric [La(COT)I(thf)$_3$] was observed. Thus, it seems likely that in our case, a dimeric species was formed in the first step of THF abstraction, which then prevented further reactivity with the dmpe. To test this assumption, we thoroughly washed the obtained precipitate with toluene (6×) and dissolved the remaining solid in THF-d_8. The $^{31}P\{^1H\}$ NMR spectrum of the THF-d_8 solution only showed a very small signal for dmpe, corresponding to 4% of the total dmpe amount, indicating that most of the dmpe had not reacted and been washed off. A signal for the COT^{2-} ligand was observed as well, indicating that the toluene-insoluble precipitate contained a lanthanum complex with COT^{2-} ligand. Additionally, we investigated the collected toluene wash solutions by $^{31}P\{^1H\}$ NMR and found that as anticipated, the majority of the dmpe had been washed out with the toluene washes. We therefore concluded that most likely the dimeric species had formed, which is highly insoluble in toluene and does not react with dmpe.

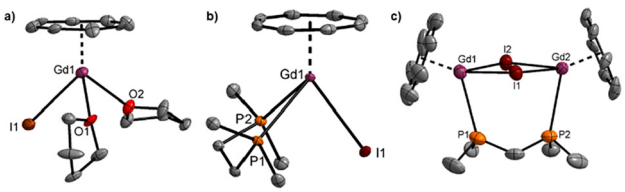

Fig. 2 Molecular structures of (a) [Gd(COT)I(thf)$_2$] (**1**), (b) [Gd(COT)I(dmpe)] (**2**) and (c) [{Gd(COT)(μ-I)}$_2$(μ-dmpm)] (**3**) in the solid state. For **1** and **2** only one of the two independent molecules in the asymmetric unit are shown. Hydrogen atoms and disorders of the COT ligands are omitted for clarity. Ellipsoids are drawn at the 50% probability level. Colour code: carbon grey, iodine maroon, gadolinium purple, oxygen red, phosphorus orange. Bond lengths and angles can be found in the SI.

Reaction of gadolinium complex **1** with dmpe and dmpm in refluxing toluene yielded the first gadolinium complexes with neutral phosphines, [Gd(COT)I(dmpe)] (**2**) and [{Gd(COT)(μ-I)}$_2$(μ-dmpm)] (**3**). Due to the strong paramagnetism of Gd, the ^{1}H NMR spectra showed only broad signals and no resonances were observed in the $^{31}P\{^1H\}$ NMR spectra, indicating close proximity of the phosphines to gadolinium. Single

crystals suitable for crystallographic analysis were obtained by slow cooling of the hot reaction solutions on NMR scale or on preparative scale by storing a concentrated solution overnight (**2**) or vapor diffusion of pentane into a toluene solution (**3**). X-ray diffraction analysis revealed a monomeric structure for **2**, in which dmpe acts as a chelating ligand, and a dimeric complex for **3**, where dmpm is a bridging ligand between the two gadolinium ions (Fig. 2b and c).

Complex **2** crystallises with two molecules in the asymmetric unit and is isostructural to its erbium homologue [Er(COT)I(dmpe)] with a three-legged piano-stool structure.[29] The Gd–P bond lengths (2.9965(9)/3.0205(9) and 3.0139(9)/3.0273(9) Å) are slightly longer compared to the Er–P bonds of 2.953 and 2.965 Å, which corresponds well to the approximately 0.05 Å larger ionic radius. The only other crystallographically characterised gadolinium–phosphine bonds are slightly shorter (2.965(1) and 2.967(1) Å) compared to the ones in **2**, potentially indicating a weaker interaction in **2**.[8] However, a direct comparison is difficult, as in the reported structure the phosphine is part of an anionic and stiff anilidophosphine ligand.

From the reaction of **1** with the smaller bite-angle bisphosphine dmpm, the dinuclear gadolinium complex [{Gd(COT)(μ-I)}$_2$(μ-dmpm)] (**3**) was obtained, in which two iodo and one dmpm ligand are bridging the two gadolinium ions (Fig. 2c). The COT^{2-} ligands cap the gadolinium ions, resulting in a distorted three-legged piano-stool geometry around the metal centers. The same structural motif was observed by Rinehart and co-workers for the related reactions of [Er(COT)I] with the sterically more demanding bis(diphenylphosphino) ethane (dppe) and bis(diphenylphosphino)methane (dppm).[29] The Gd–P bond lengths in **3** (3.017(6) and 3.021(6) Å) are only very slightly longer compared to the monomeric complex **2**. This contrasts with the erbium analogues, where the Er–P bond lengths in the dimeric complexes are elongated by up to 0.1 Å, probably due to the increased steric demand of the phenyl groups compared to methyl groups on the phosphine.

Magnetic properties of [{Gd(COT)(μ-I)}$_2$(μ-dmpm)] (3)

The magnetic properties of **3** were investigated with SQUID magnetometry (Fig. 3). At room temperature, a $\chi_M T$ value of 15.66 cm^3 K mol^{-1} is observed, which matches well with the expected $\chi_M T$ values of 15.75 cm^3 K mol^{-1} for Curie paramagnetism of two uncoupled Gd^{3+} ions.[47] The $\chi_M T$ values decrease linearly when the temperature is lowered until approximately 20 K. This behaviour can be explained by a temperature independent paramagnetism (TIP). Below 20 K, $\chi_M T$ decreases drastically, indicating weak antiferromagnetic coupling between two Gd^{3+} ions. The obtained data were analysed utilising a spin-Hamiltonian for exchange interaction and Zeeman splitting (eqn (1)):

$$\hat{H} = -2J\hat{S}_1\hat{S}_2 + g\mu_B\vec{B}(\vec{S}_1 + \vec{S}_2) \quad (1)$$

A Landé factor of 1.97, a weak antiferromagnetic coupling of −0.065 cm^{-1} and a TIP of 1520 × 10^{-6} cm^3 mol^{-1} are the best fit parameters. The obtained small coupling constant is in the same range as previously reported gadolinium complexes featuring two bridging chloride or bromide ligands (Cl: −0.0035 to −0.09 cm^{-1}, Br: −0.029 cm^{-1}).[48–52] Complex **3** also completes the series of magnetically investigated double halide bridged Gd(III) dimers, representing the first magnetic characterisation of an iodide bridged Gd(III) dimer.

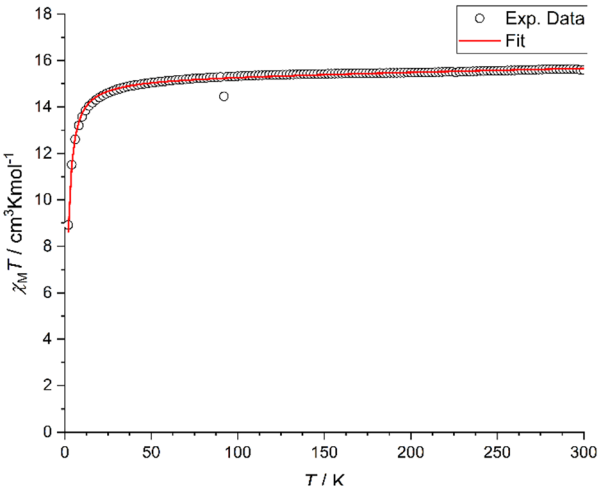

Fig. 3 Plot of $\chi_M T$ *vs.* T for **3**. The solid red line represents the calculated curve fit (see text).

Synthesis and characterisation of Cp$^-$-supported lanthanoid complexes

After the successful synthesis of the COT^{2-}-supported gadolinium phosphine complexes, we sought to investigate the ability of the smaller cyclopentadienyl ligand to support lanthanoid phosphine complexes with bidentate phosphine ligands. Additionally, we anticipated that the well-established reactivity of [LnCp$_n$] with various Lewis bases[53] and the formation of La–P bonds in a lanthanum complex with Cp$^-$-tethered phosphines in THF[16] would allow for the isolation of a lanthanum complex with a phosphine ligand in contrast to the presumable dimerisation of the donor-free lanthanum COT^{2-} precursor. We followed a similar approach as for the COT^{2-}-supported complexes through abstracting the coordinated THF from [{GdCp$_2$(thf)}$_2$(μ-Cl)$_2$] with the stronger Lewis base AlMe$_3$ in toluene and reacting the *in situ* generated solvent-free GdCp$_2$Cl with dmpe (Scheme 2a). The ^{31}P{^{1}H} NMR spectrum of the reaction mixture showed a very broad signal at approximately −52 ppm, indicating an interaction between the paramagnetic Gd^{3+} ion and the phosphine. Crystal structure determination of single crystals obtained *via* slow cooling of the reaction solution revealed that a ligand redistribution has occurred and two GdCp$_3$ fragments are bridged by one dmpe ligand forming the dimeric complex [{GdCp$_3$}$_2$(μ-dmpe)] (**4**) (Fig. 4a). The Gd–P bond lengths in **4** (2.9515(12) Å and 2.9799(8) Å) are slightly shorter compared to the ones in the COT^{2-}-supported complexes **2** and **3**, but still in the same range as for the other two previously reported complexes with Gd–PR$_3$ bonds (2.965(1) and 2.967(1) Å).[8]

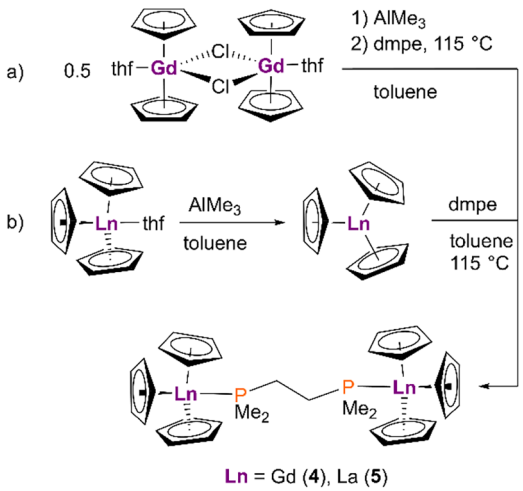

Scheme 2 Synthesis of dmpe-bridged dimeric complexes [{$LnCp_3$}$_2$(μ-dmpe)], Ln = Gd (**4**), La (**5**) by THF abstraction from [{$GdCp_2$(thf)}$_2$(μ-Cl)$_2$] (a) or [$LnCp_3$(thf)] (b) with $AlMe_3$ and subsequent reaction with dmpe.

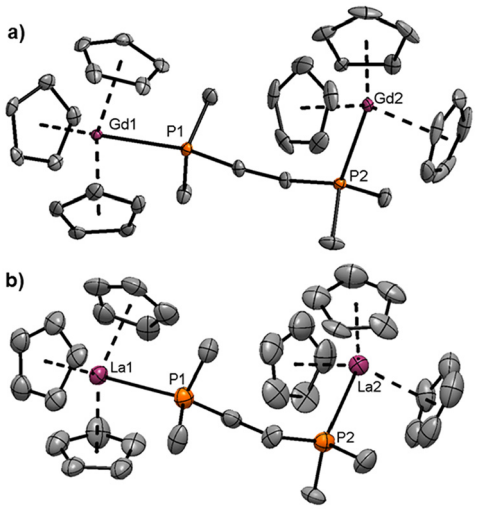

Fig. 4 Molecular structures of (a) [{$GdCp_3$}$_2$(μ-dmpe)] (**4**) and (b) [{$LaCp_3$}$_2$(μ-dmpe)] (**5**) in the solid state. Hydrogen atoms are omitted for clarity. Ellipsoids are drawn at the 50% probability level. Colour code: carbon grey, lanthanum and gadolinium purple, phosphorus orange. Bond lengths and angles can be found in the SI.

The magnetic measurement of **4** reveals two non-interacting S = 7/2 ions, as expected from the bridging dmpe ligand with an aliphatic ethylene moiety (SI Fig. SI-16). The reverse reaction of $GdCp_3$ with $GdCl_3$ to form $GdCp_2Cl$ has been observed at room temperature in THF previously,[54] suggesting that in the less polar solvent toluene and at higher temperatures the equilibrium is shifted towards $GdCp_3$. Consequently, **4** can also be obtained from the reaction of *in situ* generated [$GdCp_3$] with dmpe (Scheme 2b).

For the reaction of $LaCp_3$ with dmpe, in the $^{31}P\{^1H\}$ NMR spectrum of the reaction mixture the phosphine signal was observed at −47.4 ppm, very close to that of free dmpe. The ^1H NMR of the reaction mixture showed signals for the Cp^- ligands and dmpe. The integrals indicate that the reaction mixture still contains a large amount of free dmpe (approx. 18-fold excess of free dmpe; SI Fig. SI-7). Crystals suitable for single crystal X-ray diffraction were grown by pentane vapor diffusion into the hot-filtered reaction solutions after cooling. While the isolated single-crystalline yield was rather low (6%), powder XRD analysis of the precipitate obtained during the formation of **5** showed that complex **5** is formed in high yield (91%) and selectivity (see SI Fig. SI-16). This is in contrast to **4**, where the bulk material was found to contain Gd by ICP-OES analysis, but in too low stoichiometry. Powder XRD analysis showed only very few reflections, indicating that one or more Gd-containing side products are formed. This could be caused by the size difference of La and Gd, with the coordination sphere around the smaller Gd becoming more crowded. For **5**, only twinned crystals could be obtained, but a structure solution and refinement was still possible and showed that the dimeric complex [{$LaCp_3$}$_2$(μ-dmpe)] (**5**) was obtained (Fig. 4b), which is isostructural to **4**. The bridging coordination of dmpe between two f-elements has previously only been reported for uranium(III) in the isostructural [{UCp_3}$_2$(μ-dmpe)], for uranium(IV) in [{$U(ODipp)_4$}$_2$(μ-dmpe)] and europium(II) in [{$Eu(TeSi(SiMe_3)_3)_2(dmpe)_2$}$_2$(μ-dmpe)].[27,55,56] The structurally most related lanthanoid(III) complex is [$YbCp^*_2Cl$(dmpe)], where dmpe acts as a monodentate ligand.[24] In the only other two structurally characterised dmpe complexes of lanthanoids, monomeric complexes with dmpe as chelating ligand are observed (Fig. 1b).[26,29] Geometry optimisations using DFT with either PBE or B3LYP functionals and ZORA-def2-TZVP(P, C, H)/SARC-ZORA-TZVP(La) basis sets of a hypothetical monomeric [$LaCp_3$(dmpe)] with dmpe in a chelating coordination mode converged to a structure with dmpe as a monodentate ligand. This suggests that the steric demand of three Cp^- and two phosphine ligands is too large, leading to a bridging coordination mode in contrast to the chelating coordination observed in **2**.

The La–P bond lengths in **5** (La1–P1: 3.089(10) Å, La2–P2: 3.125(6) Å) are shorter than the La–P bond lengths in the only other known lanthanum dmpe complex (La–P: 3.143(2)–3.216(2) Å), which could be attributed to a monodentate coordination in complex **5** in contrast to a chelating coordination of dmpe in the reported complex.[26] The La–P bond lengths in other reported lanthanum complexes with tertiary phosphine-containing ligands are in the range of 3.039(2)–3.481(2) Å.[8,10,15,18,32,57–59] In addition to the characterisation in the solid state, we attempted to investigate lanthanum complex **5** in solution *via* NMR spectroscopy. However, due to very poor solubility of isolated **5** in toluene-d_8, no signals could be observed in the $^{31}P\{^1H\}$ NMR spectrum and the poor signal-to-noise ratio in the ^1H NMR spectrum precluded assignment of signals.

From the reactions of $LnCp_3$ with dmpm, only inconclusive $^{31}P\{^1H\}$ and ^1H NMR spectra were obtained for both La and Gd. Despite repeated attempts, no crystalline material could be obtained.

Table 1 Experimental and calculated Ln–P bond lengths in Å, formal shortness ratios (FSR) as well as QTAIM metrics obtained for the Ln–P BCPs in **2**, **3**, **4** and **5**. Values are in a.u. for the electron density (ρ), energy density (H), Laplacian ($\nabla^2\rho$), ellipticity (ε) at the Ln–P BCP and the delocalisation index δ(Ln,P)

		d_{exp}(Ln–P)	d_{calc}(Ln–P)	FSR	ρ	H	$\nabla^2\rho$	ε	δ(Ln,P)
2	Gd1–P1	2.9965(9)	2.982	1.099	0.032	−0.003	0.058	0.072	0.58
	Gd1–P2	3.0139(9)	3.019	1.112	0.034	−0.004	0.062	0.067	0.51
3	Gd1–P1	3.017(6)	3.000	1.106	0.033	−0.004	0.060	0.042	0.61
	Gd2–P2	3.021(6)	3.006	1.108	0.033	−0.004	0.060	0.042	0.61
4	Gd1–P1	2.9515(12)	2.917	1.075	0.038	−0.005	0.068	0.003	0.74
	Gd2–P2	2.9799(8)	2.963	1.092	0.035	−0.004	0.064	0.020	0.63
5	La1–P1	3.088(10)	3.066	1.099	0.034	−0.004	0.056	0.001	0.58
	La2–P2	3.124(6)	3.090	1.107	0.032	−0.003	0.054	0.012	0.49

Ln–P bonding

To gain further insights into the nature of the lanthanoid–phosphine bonds, quantum chemical bonding analysis of the complexes **2–5** was performed. First, the geometries were optimised starting from the crystal structures. Subsequent frequency calculations confirmed all obtained structures to be minima. A comparison of the calculated with the experimental Ln–P bond lengths showed good agreement with a slight underestimation of 0.01–0.03 Å (Table 1). Overlays of the computed and crystallographically obtained structures also showed a good agreement.

Inspection of the molecular orbitals showed purely σ-type bonding and no Ln → P π-backbonding, which is expected for the generally high ionic bonding character of lanthanoid-ligand bonds (SI Fig. SI-17–SI-20). A Quantum Theory of Atoms in Molecules (QTAIM) analysis showed bond critical points (BCPs) for all Ln–P linkages, indicating bonding interactions in all complexes. Plots of the Laplacians of the electron density showed that the interaction is as expected for a phosphine a dative P → Ln bond (Fig. 5, SI Fig. SI-21 and SI-22).

Table 1 lists selected QTAIM metrics for the Ln–P BCPs. The electron density ρ and energy density H at the BCP are commonly used as measures for covalency of a bond, with $\rho > 0.2$ and $H < 0$ indicating a covalent bond. More negative values of H are associated with a larger degree of covalency. $\rho < 0.1$ is typical for closed shell interactions. The Laplacian of the electron density $\nabla^2\rho$ is negative for strong covalent bonds.[60,61]

The energy density H is slightly negative (−0.003 to −0.005) with the Laplacians just above 0 (0.054 to 0.068) for all Ln–P bonds, indicating very weakly covalent bonding. The bond ellipticities ε are a measure for the distribution of electron density along the Ln–P bond: a value of 0 indicates completely symmetric distribution (*i.e.* a single or triple bond) and a value of 1 indicates an asymmetric distribution as would be expected for a double bond. The obtained values of 0.001–0.072 indicate a single bond for all Ln–P interactions, as expected from the molecular orbitals. The bond delocalisation index δ(Ln,P) indicates the amount of electron pair sharing and is thus a measure of bond order. With δ(Ln,P) in the range of 0.49 to 0.74, the Ln–P bonds in all complexes can be classified as single bonds.

While the general information from QTAIM on the nature of the Ln–P bonds is as expected, we were curious if the variations in bond metrics for the seemingly similar Ln–P bonds can be explained. To compare Ln–P bonds of the different metals, we therefore calculated the formal shortness ratios (FSR) as defined by Cotton:[62]

$$\mathrm{FSR_{AB}} = \frac{d_{AB}}{R_1^A + R_1^B}$$

where d_{AB} is the Ln–P bond length and R_1 are the metallic radii by Pauling.[63]

The calculated FSRs (Table 1) are in the narrow range of 1.075 to 1.112, which is at the lower end of the range of other Ln–P bonds with neutral phosphines (1.051–1.153), indicating stronger bonding.[24–29]

Plotting the different QTAIM metrics against the FSR reveals the general trend that with lower FSR values the bond becomes more covalent, as for example indicated by the increased delocalisation index (Fig. 6; see SI Fig. SI-24–SI-26 for correlation plots with ρ, H and Laplacian). This can be understood in the orbital overlap picture of covalency: a stronger shortening of the Ln–P bond leads to better orbital overlap between the Ln and P and thus a larger degree of delocalisation of the shared electrons.

While the number of data points in this study is still low and only includes two lanthanoids, one type of phosphine

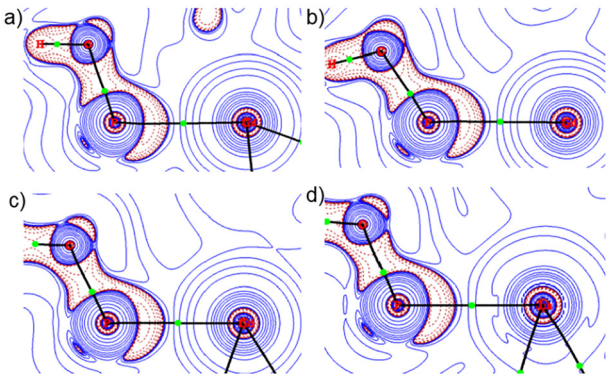

Fig. 5 Contour plots of the Laplacians of (a) **2**, (b) **3**, (c) **4** and (d) **5** in one of the Ln–P–C planes each. BCPs are denoted as green dots, black lines represent molecular graphs, positive values of the Laplacian (charge depletion) are depicted as solid blue lines, and negative values (charge accumulation) as broken red lines.

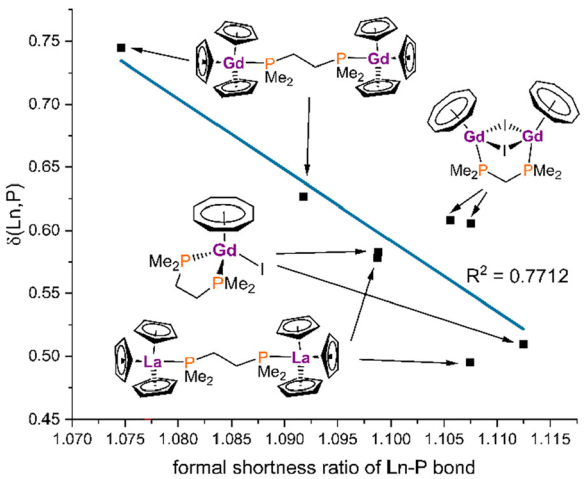

Fig. 6 Plot of the values for the delocalisation index of the Ln–P bond δ(Ln,P) against the Ln–P FSR.

ligand and Cp^-, COT^{2-} and iodide as ancillary ligands, it gives some first insights into trends in Ln–P bonding. However, more data points will be necessary to draw a conclusion for all lanthanoid phosphine complexes.

Conclusions

Utilising solvent-free precursors, four new lanthanoid complexes with neutral tertiary phosphine ligands were synthesised. Out of these, the three gadolinium complexes represent the first examples of gadolinium complexes with neutral phosphine ligands, with only one previously reported gadolinium complex with an anilidophosphine ligand. Using COT^{2-} as ancillary ligand enabled the isolation of both monomeric [Gd(COT)I(dmpe)] (**2**) with dmpe as chelating ligand and dimeric [{Gd(COT)(μ-I)}$_2$(μ-dmpm)] (**3**) where dmpm bridges the two Gd. For lanthanum however, the analogous complexes remained elusive, presumably due to dimerisation of the THF-free precursor. With Cp^- as ancillary ligands, the reaction with dmpe lead to isolable dimeric complexes [{LnCp$_3$}$_2$(μ-dmpe)] (Ln = Gd (**4**) and La (**5**)). These are the first two examples for lanthanoid(III) complexes with dmpe as a bridging ligand. The observed bridging mode is in contrast to the COT^{2-}-supported Gd complex **2**, where dmpe acts as a chelating ligand. These differences are most likely due to steric congestion around the metal in the [LnCp$_3$] fragments. SQUID measurements showed a weak antiferromagnetic coupling between the Gd^{3+} ions in **3**, which is as expected due to the bridging iodides, while no coupling was observed in **4**.

Quantum chemical bonding analysis of the Ln–P bonds confirmed the mostly ionic nature of these bonds with only a small covalent character. Nonetheless, a correlation between the Ln–P bond lengths in complexes with monodentate phosphine coordination and covalency was found, indicating that the ligand sterics can influence the degree of covalency.

The poor solubility of the isolated complexes precluded further characterisation in solution. Thus, we will modify the ancillary ligands to allow for additional solution studies in the future and to extend our studies towards the later lanthanoids.

Experimental details

General experimental details

All experiments were conducted under inert conditions of dry argon 5.0, either using a GS Mega E-Line or MBraun Unilab Plus glovebox or Schlenk techniques. All glassware was dried by heating in an oven at 120 °C overnight and in part additionally flame dried and cooled *in vacuo*.

Materials

Hexane and toluene were dried by using an MBraun solvent purification system, degassing and subsequently storing over 4 Å molecular sieves for at least five days prior to use. Pentane and THF were dried by distillation from potassium. Deuterated solvents were purchased from Deutero and dried by storage over 4 Å molecular sieves. All solvents were degassed either by three cycles of freeze–pump–thaw or sparging with argon. Gadolinium powder, $LaCl_3$ and $GdCl_3$ were purchased from abcr and cyclooctatetraene was purchased from TCI. Dicyclopentadiene, 1,2-(dimethylphosphino)methane, 1,2-(dimethylphosphino)ethane and 2.0 M trimethylaluminum in toluene were purchased from Sigma Aldrich. Iodine was purchased from J. T. Baker and sublimed *in vacuo* before use. Cyclooctatetraene was stored over 4 Å molecular sieves and the remaining chemicals were used as purchased. [GdI$_3$(thf)$_{3.5}$],[39] NaCp,[64] [{GdCp$_2$(thf)}$_2$(μ-Cl)$_2$],[54] [GdCp$_3$(thf)][65] and [LaCp$_3$(thf)][65] were prepared according to reported procedures. Purification of the lanthanoid-Cp complexes was performed by filtering the reaction solutions, reducing the volume *in vacuo* and storing at −30 °C to precipitate the products.

Methods

NMR spectroscopy. NMR spectra were recorded on a Bruker Avance Neo 400, or a Bruker Avance III HD 500 referenced against the residual solvent signal of the deuterated solvents.

Elemental analysis. Elemental combustion analysis (CHN) of the samples was conducted by the analytical laboratory of the University of Göttingen on an elementar 4.1 vario EL III and showed a systematic deviation to lower carbon values for measurements of various samples across different research groups.

IR spectroscopy. ATR-IR spectra were recorded from solid samples with an Agilent Cary 630 FTIR Spectrometer inside of an argon glovebox.

Magnetometry. Temperature-dependent magnetic susceptibility measurements were carried out with a Quantum-Design MPMS3 SQUID magnetometer equipped with a 7 Tesla magnet in the range from 300 to 2.0 K at a magnetic field of 0.5 T. The powdered samples were contained in a polycarbonate capsule and fixed in a non-magnetic sample holder. Each raw data file

for the measured magnetic moment was corrected for the diamagnetic contribution of the polycarbonate capsule according to $M^{dia}(capsule) = \chi_g \cdot m \cdot H$, with an experimentally obtained gram susceptibility of the polycarbonate capsule. The molar susceptibility data were corrected for the diamagnetic contribution according to $\chi_M^{dia}(sample) = -0.5 \times M \times 10^{-6}$ cm^3 mol^{-1}.[66] Experimental data were modelled with the Dave program[67] using a fitting procedure to the spin Hamiltonian (eqn (1); $J = 0$ for **4**). Temperature-independent paramagnetism (TIP = 1520 × 10^{-6} cm^3 mol^{-1} for **3**) was included according to $\chi_{calc} = \chi + TIP$.

Crystallographic studies. Single crystal data and details of the data collections are given in SI Tables SI-1 and SI-2, molecular structures are shown in Fig. 2 and 4. Single crystal X-ray data were collected on a BRUKER D8-QUEST diffractometer (monochromated Mo-Kα radiation, λ = 0.71073 Å) by use of ω or ω and ϕ scans at low temperature. The structures were solved with SHELXT and refined on F^2 using all reflections with SHELXL.[68,69] Non-hydrogen atoms were refined anisotropically. Hydrogen atoms were placed in calculated positions and assigned to an isotropic displacement parameter of 1.5/1.2$U_{eq.}$(C).

In case of **3** the COT^{2-} ligand bound to Gd2 was found to be disordered about two positions (occupancy factors: 0.49(2)/0.51(2)) and was refined using SAME and RIGU restraints and EADP constraints. In case of **4** one Cp^- ring (bound to Gd2) was found to be disordered about two positions (occupancy factors: 0.720(13)/0.280(13)) and was refined using RIGU restraints and EADP constraints. Crystals of **1** and **5** were found to be twinned (twin law **1**: −1 0 0, −0.047 1 −0.043, 0 0 −1; twin law **5**: −0.906 0 0.188, 0 −0, 0.953 0 0.906). RIGU restraints for all atoms in **1** and for carbon atoms in **5** were applied. BASF were refined to 0.211(3) and 0.373(4) for **1** and **5**. Absorption corrections were performed by the multi-scan method with SADABS.[70]

The powder diffraction pattern measurements were carried out with Panalytical MPD X'Pert Pro diffractometer in the Bragg–Brentano geometry. The sample was protected from air and moisture with a Kapton Polyimide foil. The Cu Kα radiation was not monochromated. The measurements were performed at room temperature in continuous scan mode over the angular range of $4.5 \leq 2\theta \leq 60°$ with a step size of 0.0131°. φ was set to 138.7°. The measurement time was 21 minutes and the counting time was 72.420 s.

Syntheses of compounds

[Gd(COT)I(thf)$_2$] (1). Potassium cyclooctatetraenide was synthesised following a procedure of Wayda *et al.* (52.7 mg; 56.97 µL; 0.51 mmol cyclooctatetraene; 39.6 mg; 1.02 mmol K).[71] The reaction mixture of K_2COT was then slowly added to a stirring suspension of [GdI$_3$(thf)$_{3.5}$] (400 mg; 0.51 mmol) in THF (15 mL). After 24 h the reaction mixture was heated to reflux for 1 h and filtered hot. Reducing the yellow solution *in vacuo* and storage at −30 °C yielded **1** as colourless fine needles (55%; 149 mg; 0.28 mmol) suitable for single crystal X-ray diffraction. IR (band assignment and spectra in the SI): ν (cm^{-1}) 2951 w, 2891 w, 1607 w, 1454 w, 1365 w, 1342 w, 1309 w, 1247 w, 1176 w, 1012 m, 893 m, 859 m, 772 w, 748 m, 705 s, 667 m. CHN ($C_{16}H_{24}GdIO_2$): calcd C 36.09, H 4.54; found: C 35.12, H 4.47.

[Gd(COT)I(dmpe)] (2). Method A: To a suspension of [(COT)GdI(thf)$_2$] (20 mg; 37.6 µmol) in toluene, $AlMe_3$ in toluene (1 mL of a 2.0 M solution) was added. The suspension was stirred overnight, after which the mother liquor was decanted off. The solid was washed once with 3 mL of toluene and then dried *in vacuo*. The powder was placed in a J. Young NMR tube, suspended in toluene-d_8 (0.6 mL) and dmpe (5.65 mg; 37.6 µmol) was added. The suspension was heated for 6 h to reflux and frequently mixed up. Afterwards, the mixture was cooled slowly to yield **2** as green X-ray quality crystals.

Method B: To a suspension of [(COT)GdI(thf)$_2$] (48.0 mg; 90.1 µmol) in toluene (5 mL), $AlMe_3$ in toluene (1 mL of a 2.0 M solution) was added, and the suspension was stirred for 24 h. The mother liquor was decanted off and the yellow solid was washed twice with toluene (5 mL). Afterwards the solid was suspended in toluene (30 mL) and dmpe (13.5 mg; 15.0 µL; 90.0 µmol) was added. The yellow solution was heated to 115 °C for 1 h. Afterwards the reaction mixture was filtered hot, and the volume was reduced *in vacuo*. Green crystals of **2** were obtained by storing the solution at room temperature overnight (46%; 22.1 mg; 41.4 µmol). NMR: the strong paramagnetism of Gd precludes the assignment of observed signals. ^{1}H NMR (300 MHz, toluene-d_8): 5.73 (b), 3.05 (b), 1.30 (b), 0.46 (b), −13.78 (b). ^{31}P{^{1}H} (121.5 MHz, toluene-d_8): no resonance observed. IR (band assignment and spectra in the SI): ν (cm^{-1}) 3039 w, 2960 w, 2891 w, 1545 w, 1420 m, 1303 w, 1260 m, 1143 w, 1094 m, 1012 m, 945 m, 928 m, 891 m, 869 m, 796 m, 768 m, 746 m, 731 m, 695 s. CHN ($C_{14}H_{24}GdIP_2$): calcd C 31.23, H 4.49; found: C 30.59, H 4.42.

[{Gd(COT)(µ-I)}$_2$(µ-dmpm)] (3). Method A: To a suspension of [(COT)GdI(thf)$_2$] (20 mg; 37.6 µmol) in toluene, $AlMe_3$ in toluene (1 mL of a 2.0 M solution) was added. The suspension was stirred overnight, after which the mother liquor was decanted off. The solid was washed once with 3 mL of toluene and then dried *in vacuo*. The powder was placed in a J. Young NMR tube, suspended in toluene-d_8 (0.6 mL) and dmpm (5.12 mg; 37.6 µmol) was added. The suspension was heated for 6 h to reflux and frequently mixed up. Afterwards the mixture was cooled slowly to yield **3** as green X-ray quality crystals.

Method B: To a suspension of [(COT)GdI(thf)$_2$] (88.0 mg; 0.17 mmol) in toluene (5 mL), $AlMe_3$ in toluene (1 mL of a 2.0 M solution) was added, and the suspension was stirred for 24 h. The mother liquor was decanted off and the yellow solid was washed twice with toluene (5 mL). Afterwards the solid was suspended in toluene (50 mL) and dmpm (16.9 mg; 19.6 µL; 0.12 mmol) was added. The yellow suspension was heated to 115 °C for 3 h. Afterwards, the reaction mixture was filtered hot and green crystals of **3** were grown from a vapor diffusion of pentane in the solution (26%; 20.2 mg; 22.1 µmol). NMR: due to the strong paramagnetism of Gd not all expected resonances could be observed. ^{1}H (300 MHz,

toluene-d_8): 8.27 (b), 7.15 (b), 6.40 (b), 3.35 (b), 0.69 (b), −0.23 (b). $^{31}P\{^1H\}$ (121.5 MHz, toluene-d_8): no resonance observed. IR (band assignment and spectra in the SI): ν (cm^{-1}) 3087 w, 2964 w, 2902 w, 1495 w, 1415 m, 1359 w, 1284 m, 1262 m, 1096 m, 1016 m, 951 m, 930 m, 893 m, 798 m, 768 m, 748 m, 725 w, 701 s. CHN ($C_{21}H_{30}Gd_2I_2P_2$): calcd C 27.63, H 3.31; found: C 24.45, H 3.26.

[{GdCp$_3$}$_2$(μ-dmpe)] (4). Method A: To a suspension of [{GdCp$_2$(thf)}$_2$(μ-Cl)$_2$] (13 mg; 32.9 μmol) in toluene, $AlMe_3$ in toluene (1 mL of a 2.0 M solution) was added. The suspension was stirred overnight, after which the mother liquor was decanted off. The solid was washed once with 3 mL of toluene and then dried *in vacuo*. The powder was placed in a J. Young NMR tube, suspended in toluene-d_8 (0.6 mL) and dmpe (4.94 mg; 32.9 μmol) was added. The suspension was heated for 6 h to reflux and frequently mixed up. Afterwards, the mixture was cooled slowly to yield **4** as colourless X-ray quality crystals.

Method B: To a suspension of [GdCp$_3$(thf)] (77 mg; 0.18 mmol) in toluene (4 mL), $AlMe_3$ in toluene (1 mL of a 2.0 M solution) was added, and the suspension was stirred for 24 h. The mother liquor was decanted off and the yellow solid was washed twice with toluene (5 mL). Afterwards, the solid was suspended in toluene (50 mL) and dmpe (20.4 mg; 22.7 μL; 0.13 mmol) was added. The suspension was heated to 115 °C for 6 h turning from slightly yellow to colourless. The reaction mixture was filtered hot and **4** was obtained as colourless crystals from vapor diffusion of pentane into the solution (17%; 13.4 mg; 15.7 μmol). The identity of the filter cake could not be determined reliably. CHN analysis of the filter cake did not match **4**. ICP-OES measurement showed the presence of Gd, but the nature of the Gd compound could not be established.

NMR: Due to the strong paramagnetism of Gd, only very broad signals are observed. ^1H (300 MHz, toluene-d_8) 3.51 (b), 2.19 (b), 0.33 (b). $^{31}P\{^1H\}$ (121.5 MHz, toluene-d_8) −52.1 (b) ppm. IR (band assignment and spectra in the SI): ν (cm^{-1}) 3074 w, 2908 w, 1642 w, 1419 w, 1286 w, 1189 w, 1115 w, 1059 w, 1008 m, 941 m. 902 m, 841 w, 749 s. CHN ($C_{36}H_{46}Gd_2P_2$): calcd C 50.56, H 5.42; found: C 48.88, H 5.32.

[{LaCp$_3$}$_2$(μ-dmpe)] (5). To a suspension of [LaCp$_3$(thf)] (76 mg; 0.19 mmol) in toluene (2 mL), $AlMe_3$ in toluene (1 mL of a 2.0 M solution) was added, and the suspension was stirred for 24 h. The mother liquor was decanted off, and the white solid was washed twice with toluene (4 mL). Afterwards, the solid was suspended in toluene (40 mL) and dmpe (21.1 mg; 23.4 μL; 0.14 mmol) was added. The suspension was heated to 115 °C for 6 h, filtered hot and colourless low X-ray quality crystals were obtained from vapor diffusion of pentane in the solution (6%; 5 mg; 6.1 μmol).

Larger scale. Procedure as above but using 145 mg (0.35 mmol) of [LaCp$_3$(thf)], 1.5 mL $AlMe_3$ in toluene (2.0 M) and 33 mg dmpe (0.22 mmol) in 10 mL toluene. The reaction mixture was filtered hot, and the remaining filter cake was dried under vacuum. Yield: 135 mg (91%; 0.16 mmol) of microcrystalline **5**. NMR: isolated **5** was too insoluble in toluene-d_8 for a meaningful NMR characterisation. IR (band assignment and spectra in the SI): ν (cm^{-1}) 3081 w, 2906 w, 1637 w, 1506 w, 1422 w, 1286 w, 1187 w, 1113 w, 1059 w, 1007 m, 941 m, 893 m, 746 s. pXRD: matches with simulated pXRD from single crystal diffraction data (see SI Fig. S16). CHN analysis: inconclusive results with large variations between measurements.

Computational details

Geometry optimisations and subsequent analytical frequency calculations for confirmation of minima were carried out with Orca 5.0.4 starting from the experimentally obtained crystal structures.[72–74] All structures were optimised with the PBE functional and ZORA-def2-TZVP basis set.[75,76] For lanthanum, gadolinium and iodine, the SARC-ZORA-TZVP basis set was used.[77] Scalar relativistic effects were taken into account by using the zero order relativistic approximation (ZORA).[78–80] Dispersion corrections were included using Grimme's D3 dispersion correction with Becke–Johnson damping.[81,82] Quantum Theory of Atoms in Molecules (QTAIM) analysis and the generation of plots of the Laplacian of the electron density was done with multiWFN using the Orca-generated wfx files.[83] Structures and molecular orbitals were visualised with Chemcraft.[84]

Author contributions

J. L.: conceptualisation, investigation, visualisation, writing – original draft, S. J. G.: investigation, formal analysis, visualisation; C. Z.: investigation, S. Dechert: investigation, formal analysis, writing – review & editing, S. Demeshko: investigation, formal analysis, writing – review & editing, L. V.: conceptualisation, investigation, formal analysis, funding acquisition, visualisation, writing – original draft, writing – review & editing, project administration.

Conflicts of interest

There are no conflicts to declare.

Data availability

The data supporting this article have been included as part of the supplementary information (SI). Supplementary information: NMR spectra, IR spectra, crystallographic data, powder crystallographic data, SQUID data, Fig. SI-18 to SI-21 (plots of molecular orbitals), Fig. SI-22 and SI-23 (plots of Laplacians), Fig. SI-24 to SI-26 (correlation plots), coordinates of DFT optimised structures. See DOI: https://doi.org/10.1039/d6dt01324d.

CCDC 2427126–2427130 (for compounds **1–5**) contain the supplementary crystallographic data for this paper.[85a–e]

Acknowledgements

J. L. and L. V. thank Prof. Dr Franc Meyer for generous provision of lab space and facilities and general support. The high-performance computing facility of the University of Hamburg is acknowledged for computing resources and software provision on the Hummel and Hummel-2 clusters and technical support. The Hummel-2 cluster was funded by Deutsche Forschungsgemeinschaft (DFG, German Research Foundation) – 498394658. Isabelle Nevoigt is thanked for measuring the pXRD spectra. This research was funded by the Fonds der Chemischen Industrie through a Liebig fellowship to L. V. C. Z. acknowledges the Deutsche Bundesstiftung Umwelt for a Ph.D. fellowship. This project has been partly funded by the Deutsche Forschungsgemeinschaft (DFG) project number 423268549 (INST 186/1327-1 FUGG) and the Nds. Ministerium für Wissenschaft und Kultur (MWK).

References

1 J. F. Hartwig, *Organotransition Metal Chemistry: From Bonding to Catalysis*, University Science Books, Mill Valley, 2010.
2 R. Martin and S. L. Buchwald, *Acc. Chem. Res.*, 2008, **41**, 1461–1473.
3 H. U. Blaser, W. Brieden, B. Pugin, F. Spindler, M. Studer and A. Togni, *Top. Catal.*, 2002, **19**, 3–16.
4 R. D. Fischer and H. Fischer, *J. Organomet. Chem.*, 1965, **4**, 412–414.
5 E. O. Fischer and H. Fischer, *J. Organomet. Chem.*, 1966, **6**, 141–148.
6 C. Bielang and R. D. Fischer, *J. Organomet. Chem.*, 1978, **161**, 335–346.
7 D. J. Schwartz and R. A. Andersen, *Organometallics*, 1995, **14**, 4308–4318.
8 F. A. Watt, A. Krishna, G. Golovanov, H. Ott, R. Schoch, C. Wölper, A. G. Neuba and S. Hohloch, *Inorg. Chem.*, 2020, **59**, 2719–2732.
9 J. D. Masuda, K. C. Jantunen, O. V. Ozerov, K. J. T. Noonan, D. P. Gates, B. L. Scott and J. L. Kiplinger, *J. Am. Chem. Soc.*, 2008, **130**, 2408–2409.
10 A. V. Zabula, Y. Qiao, A. J. Kosanovich, T. Cheisson, B. C. Manor, P. J. Carroll, O. V. Ozerov and E. J. Schelter, *Chem. – Eur. J.*, 2017, **23**, 17923–17934.
11 P. B. Hitchcock, M. F. Lappert and I. A. MacKinnon, *J. Chem. Soc., Chem. Commun.*, 1988, **14**, 1557.
12 F. Sinclair, J. A. Hlina, J. A. L. Wells, M. P. Shaver and P. L. Arnold, *Dalton Trans.*, 2017, **46**, 10786–10790.
13 A. Haidinger, C. I. Dilly, R. C. Fischer, D. Svatunek, J. M. Uher and J. A. Hlina, *Inorg. Chem.*, 2023, **62**, 17713–17720.
14 J. Jung, C. M. Legendre, S. Demeshko, R. Herbst-Irmer and D. Stalke, *Dalton Trans.*, 2021, **50**, 17194–17201.
15 M. Dahlen, N. Reinfandt, C. Jin, M. T. Gamer, K. Fink and P. W. Roesky, *Chem. – Eur. J.*, 2021, **27**, 15128–15136.
16 H. H. Karsch, V. Graf, M. Reisky and E. Witt, *Eur. J. Inorg. Chem.*, 1998, **1998**, 1404–1406.
17 Y. Zhang, X. Pan, M. Xu, C. Xiong, D. Hong, H. Fang and P. Cui, *Inorg. Chem.*, 2023, **62**, 3836–3846.
18 B. L. Ramirez and C. C. Lu, *J. Am. Chem. Soc.*, 2020, **142**, 5396–5407.
19 L. Zhang, T. Suzuki, Y. Luo, M. Nishiura and Z. Hou, *Angew. Chem., Int. Ed.*, 2007, **46**, 1909–1913.
20 W. Miao, S. Li, D. Cui and B. Huang, *J. Organomet. Chem.*, 2007, **692**, 3823–3834.
21 H. Liu, F. You, X. Hu, Y. Huo and X. Shi, *Organometallics*, 2022, **41**, 3645–3653.
22 T. D. Tilley, R. A. Andersen and A. Zalkin, *J. Am. Chem. Soc.*, 1982, **104**, 3725–3727.
23 S. S. Rozenel and R. A. Andersen, *Inorg. Chim. Acta*, 2014, **422**, 202–205.
24 T. D. Tilley, R. A. Andersen and A. Zalkin, *Inorg. Chem.*, 1983, **22**, 856–859.
25 S. Stults and A. Zalkin, *Acta Crystallogr., Sect. C: Struct. Chem.*, 1987, **43**, 430–432.
26 D. R. Cary and J. Arnold, *J. Am. Chem. Soc.*, 1993, **115**, 2520–2521.
27 D. R. Cary and J. Arnold, *Inorg. Chem.*, 1994, **33**, 1791–1796.
28 S. Arndt, P. Voth, T. P. Spaniol and J. Okuda, *Organometallics*, 2000, **19**, 4690–4700.
29 J. D. Hilgar, M. G. Bernbeck and J. D. Rinehart, *J. Am. Chem. Soc.*, 2019, **141**, 1913–1917.
30 S. K. Thakur, N. Roig, J. Maurer, J. Langer, M. Alonso and S. Harder, *J. Am. Chem. Soc.*, 2025, **147**, 12555–12561.
31 E. Tanuhadi, A. S. Bair, M. Johnson, P. Fontaine, J. Klosin, S. Pal and P. L. Arnold, *Chem. Sci.*, 2025, **16**, 280–287.
32 L. C. H. Gerber, E. Le Roux, K. W. Törnroos and R. Anwander, *Chem. – Eur. J.*, 2008, **14**, 9555–9564.
33 K. Mashima, Y. Nakayama, A. Nakamura, N. Kanehisa, Y. Kai and H. Takaya, *J. Organomet. Chem.*, 1994, **473**, 85–91.
34 L. Münzfeld, C. Schoo, S. Bestgen, E. Moreno-Pineda, R. Köppe, M. Ruben and P. W. Roesky, *Nat. Commun.*, 2019, **10**, 3135.
35 M. Tricoire, L. Münzfeld, J. Moutet, N. Mahieu, L. La Droitte, E. Moreno-Pineda, F. Gendron, J. D. Hilgar, J. D. Rinehart, M. Ruben, B. Le Guennic, O. Cador, P. W. Roesky and G. Nocton, *Chem. – Eur. J.*, 2021, **27**, 13558–13567.
36 J. D. Hilgar, M. G. Bernbeck, B. S. Flores and J. D. Rinehart, *Chem. Sci.*, 2018, **9**, 7204–7209.
37 I. L. Fedushkin, M. N. Bochkarev, S. Dechert and H. Schumann, *Chem. – Eur. J.*, 2001, **7**, 3558.
38 K. L. M. Harriman, I. Korobkov and M. Murugesu, *Organometallics*, 2017, **36**, 4515–4518.
39 K. Izod, S. T. Liddle and W. Clegg, *Inorg. Chem.*, 2004, **43**, 214–218.
40 T. K. Panda, A. G. Trambitas, T. Bannenberg, C. G. Hrib, S. Randoll, P. G. Jones and M. Tamm, *Inorg. Chem.*, 2009, **48**, 5462–5472.

41 J. Wang, J. Smith, C. Zheng, J. A. Maguire and N. S. Hosmane, *Organometallics*, 2006, **25**, 4118–4130.
42 J. Jin, X. Zhuang, Z. Jin and W. Chen, *J. Organomet. Chem.*, 1995, **490**, C8–C13.
43 W. J. Evans, B. L. Davis, T. M. Champagne and J. W. Ziller, *Proc. Natl. Acad. Sci. U. S. A.*, 2006, **103**, 12678–12683.
44 K. Mashima and H. Takaya, *Tetrahedron Lett.*, 1989, **30**, 3697–3700.
45 U. Kilimann, M. Schäfer, R. Herbst-Irmer and F. T. Edelmann, *J. Organomet. Chem.*, 1994, **469**, C10–C14.
46 C. Meermann, K. Ohno, K. W. Törnroos, K. Mashima and R. Anwander, *Eur. J. Inorg. Chem.*, 2009, **2009**, 76–85.
47 *Molecular Magnetism: From Molecular Assemblies to the Devices*, ed. E. Coronado, P. Delhaès, D. Gatteschi and J. S. Miller, Springer Netherlands, Dordrecht, 1996.
48 A. Rasamsetty, S. Mehta, K. U. Ansari, P. Kumar, A. Mondal and M. Shanmugam, *Dalton Trans.*, 2022, **51**, 63–68.
49 T. Han, Y.-S. Ding, Z.-H. Li, K.-X. Yu, Y.-Q. Zhai, N. F. Chilton and Y.-Z. Zheng, *Chem. Commun.*, 2019, **55**, 7930–7933.
50 M. Li, H. Wu, Z. Xia, V. Montigaud, O. Cador, B. Le Guennic, H. Ke, W. Wang, G. Xie and S. Chen, *Chem. Commun.*, 2019, **55**, 14661–14664.
51 D. Lüert, A.-K. Kreyenschmidt, C. M. Legendre, R. Herbst-Irmer and D. Stalke, *Inorg. Chem.*, 2022, **61**, 5234–5244.
52 S. Deshapriya, F. Delano and S. Demir, *ChemPlusChem*, 2024, **89**, 1–9.
53 H. Schumann, J. A. Meese-Marktscheffel and L. Esser, *Chem. Rev.*, 1995, **95**, 865–986.
54 R. E. Maginn, S. Manastyrskyj and M. Dubeck, *J. Am. Chem. Soc.*, 1963, **85**, 672–676.
55 A. Zalkin, J. G. Brennan and R. A. Andersen, *Acta Crystallogr., Sect. C: Struct. Chem.*, 1987, **43**, 1706–1708.
56 P. L. Arnold, C. J. V. Halliday, L. Puig-Urrea and G. S. Nichol, *Inorg. Chem.*, 2021, **60**, 4162–4170.
57 H. H. Karsch, G. Ferazin, O. Steigelmann, H. Kooijman and W. Hiller, *Angew. Chem., Int. Ed. Engl.*, 1993, **32**, 1739–1742.
58 F. A. Watt, K. N. McCabe, R. Schoch, L. Maron and S. Hohloch, *Chem. Commun.*, 2020, **56**, 15410–15413.
59 F. A. Watt, L. Burkhardt, R. Schoch, S. Mitzinger, M. Bauer, F. Weigend, J. M. Goicoechea, F. Tambornino and S. Hohloch, *Angew. Chem., Int. Ed.*, 2021, **60**, 9534–9539.
60 D. Cremer and E. Kraka, *Angew. Chem., Int. Ed. Engl.*, 1984, **23**, 627–628.
61 C. F. Matta and R. J. Boyd, in *The Quantum Theory of Atoms in Molecules*, ed. C. F. Matta and R. J. Boyd, Wiley, 2007, pp. 1–34.
62 F. A. Cotton, C. A. Murillo and R. A. Walton, in *Multiple Bonds Between Metal Atoms*, Springer Science and Business Media, 3rd edn, 2005.
63 L. Pauling, *J. Am. Chem. Soc.*, 1947, **69**, 542–553.
64 T. K. Panda, M. T. Gamer and P. W. Roesky, *Organometallics*, 2003, **22**, 877–878.
65 R. D. Rogers, J. L. Atwood, A. Emad, D. J. Sikora and M. D. Rausch, *J. Organomet. Chem.*, 1981, **216**, 383–392.
66 O. Kahn, *Molecular Magnetism*, VCH Publishers Inc., New York, 1993.
67 R. T. Azuah, L. R. Kneller, Y. Qiu, P. L. W. Tregenna-Piggott, C. M. Brown, J. R. D. Copley and R. M. Dimeo, *J. Res. Natl. Inst. Stand. Technol.*, 2009, **114**, 341.
68 G. M. Sheldrick, *Acta Crystallogr., Sect. A: Found. Adv.*, 2015, **71**, 3–8.
69 G. M. Sheldrick, *Acta Crystallogr., Sect. C: Struct. Chem.*, 2015, **71**, 3–8.
70 *SADABS*, Bruker AXS GmbH, Karlsruhe, Germany, 2016.
71 A. L. Wayda, J. T. Rigsbee and A. Streitwieser, in *Inorganic Syntheses*, ed. A. P. Ginsberg, 1990, vol. 16, pp. 150–154.
72 F. Neese, *Wiley Interdiscip. Rev.: Comput. Mol. Sci.*, 2012, **2**, 73–78.
73 F. Neese, *Wiley Interdiscip. Rev.: Comput. Mol. Sci.*, 2018, **8**, 4–9.
74 F. Neese, F. Wennmohs, U. Becker and C. Riplinger, *J. Chem. Phys.*, 2020, **152**, 224108.
75 J. P. Perdew, K. Burke and M. Ernzerhof, *Phys. Rev. Lett.*, 1996, **77**, 3865–3868.
76 F. Weigend and R. Ahlrichs, *Phys. Chem. Chem. Phys.*, 2005, **7**, 3297–3305.
77 D. A. Pantazis and F. Neese, *J. Chem. Theory Comput.*, 2011, **7**, 677–684.
78 E. van Lenthe, E. J. Baerends and J. G. Snijders, *J. Chem. Phys.*, 1993, **99**, 4597–4610.
79 E. van Lenthe, E. J. Baerends and J. G. Snijders, *J. Chem. Phys.*, 1994, **101**, 9783–9792.
80 E. van Lenthe, A. Ehlers and E.-J. Baerends, *J. Chem. Phys.*, 1999, **110**, 8943–8953.
81 S. Grimme, S. Ehrlich and L. Goerigk, *J. Comput. Chem.*, 2011, **32**, 1456–1465.
82 S. Grimme, J. Antony, S. Ehrlich and H. Krieg, *J. Chem. Phys.*, 2010, **132**, 154104.
83 T. Lu and F. Chen, *J. Comput. Chem.*, 2012, **33**, 580–592.
84 G. A. Zhurko, *Chemcraft - graphical program for visualization of quantum chemistry computations*, Ivanovo, Russia, 2005.
85 (*a*) CCDC 2427126: Experimental Crystal Structure Determination, 2025, DOI: 10.5517/ccdc.csd.cc2mgmd4; (*b*) CCDC 2427127: Experimental Crystal Structure Determination, 2025, DOI: 10.5517/ccdc.csd.cc2mgmf5; (*c*) CCDC 2427128: Experimental Crystal Structure Determination, 2025, DOI: 10.5517/ccdc.csd.cc2mgmg6; (*d*) CCDC 2427129: Experimental Crystal Structure Determination, 2025, DOI: 10.5517/ccdc.csd.cc2mgmh7; (*e*) CCDC 2427130: Experimental Crystal Structure Determination, 2025, DOI: 10.5517/ccdc.csd.cc2mgmj8.